Efficient Spin Torques in Antiferromagnetic CoO/Pt Quantified by Comparing Field- and Current-Induced Switching

L. Baldrati,[1,*] C. Schmitt,[1] O. Gomonay,[1] R. Lebrun,[1,2] R. Ramos,[3] E. Saitoh,[3,4,5,6,7] J. Sinova,[1,8,9] and M. Kläui[1,9,†]

[1]*Institute of Physics, Johannes Gutenberg-University Mainz, 55128 Mainz, Germany*
[2]*Unité Mixte de Physique CNRS, Thales, Université Paris-Sud, Université Paris-Saclay, Palaiseau 91767, France*
[3]*WPI-Advanced Institute for Materials Research, Tohoku University, Sendai 980-8577, Japan*
[4]*Institute for Materials Research, Tohoku University, Sendai 980-8577, Japan*
[5]*Advanced Science Research Center, Japan Atomic Energy Agency, Tokai 319-1195, Japan*
[6]*Center for Spintronics Research Network, Tohoku University, Sendai 980-8577, Japan*
[7]*Department of Applied Physics, The University of Tokyo, Tokyo 113-8656, Japan*
[8]*Institute of Physics, Academy of Sciences of the Czech Republic, Praha 11720, Czech Republic*
[9]*Graduate School of Excellence Materials Science in Mainz, 55128 Mainz, Germany*

(Received 26 February 2020; revised 2 July 2020; accepted 10 July 2020; published 10 August 2020; corrected 10 March 2021)

We achieve current-induced switching in collinear insulating antiferromagnetic CoO/Pt, with fourfold in-plane magnetic anisotropy. This is measured electrically by spin Hall magnetoresistance and confirmed by the magnetic field-induced spin-flop transition of the CoO layer. By applying current pulses and magnetic fields, we quantify the efficiency of the acting current-induced torques and estimate a current-field equivalence ratio of 4×10^{-11} T A^{-1} m^2. The Néel vector final state ($\boldsymbol{n} \perp \boldsymbol{j}$) is in line with a thermomagnetoelastic switching mechanism for a negative magnetoelastic constant of the CoO.

DOI: 10.1103/PhysRevLett.125.077201

Antiferromagnetic materials (AFMs) are considered important future materials for spintronics, thanks to advantageous properties compared to ferromagnets, which potentially enable higher speed (resonance frequencies in the terahertz range), bit packing density (absence of generated stray field), and resilience to external applied magnetic fields [1]. However, exploiting AFMs in applications requires electrical reading and writing of information, which can be stored, e.g., in the orientation of the antiferromagnetic Néel vector $\boldsymbol{n}$. Recently, this has been reported by electrical measurements and direct magnetic imaging, both in metallic AFMs [2,3] and bilayers of insulating AFMs and heavy metals [4–9]. The underlying switching mechanism in the latter case is being debated, in terms of both origin and efficiency [4–7]. While different claims have been made, a key missing step is the experimental quantification of the acting torques in compensated AFMs, which enables comparison to future *ab initio* calculations. This has been prevented, so far, by the difficult reading of the antiferromagnetic state, the presence of electrical signal artefacts not related to the antiferromagnetic order [6,7,10–12], and the difficulties in controlling the orientation of $\boldsymbol{n}$ by an external magnetic field $\boldsymbol{H}$. To quantify the torques, one needs to study compensated AFMs with low anisotropy that present an accessible spin-flop transition, i.e., the reorientation from $\boldsymbol{n} \| \boldsymbol{H}$ to $\boldsymbol{n} \perp \boldsymbol{H}$.

A possible material with apt properties is CoO, a collinear compensated antiferromagnet with Néel temperature $T_{\text{Néel}} = 291$ K in the bulk [13–15], and spin-flop transition at 12 T and 77 K [16]. By growing CoO thin films under a compressive strain on MgO(001) (lattice mismatch 1.1%) [17,18], one can induce an in-plane easy magnetic configuration and $T_{\text{Néel}}$ around room temperature. In MgO//CoO/Fe thin films it was conjectured, by looking at the Fe anisotropy, that the CoO layer has fourfold in-plane anisotropy [19]. The existence of a spin-flop transition for such strained thin films with in-plane easy axes has not been investigated, but, if accessible, may prove suitable to compare current- and field-induced switching efficiencies quantitatively.

In this Letter, we quantify the torques due to current injection in the CoO/Pt system. First, we show that the compressive strain favors a fourfold in-plane magnetic anisotropy of the CoO layer with two easy axes in the (001) plane. Having two orthogonal stable states is ideal for applications where the orientation of $\boldsymbol{n}$ is read by spin Hall magnetoresistance (SMR) [5,20,21]. Second, we achieve electrical switching and probe its symmetry, showing that this switching is of magnetic origin and not related to the Seebeck effect [11] or to electromigration effects that we identify for particular conditions as well [7,10]. Finally, we directly compare the effects of the field and current pulses in a Pt layer on the reorientation of $\boldsymbol{n}$ in the CoO, quantifying the current-field equivalence of the current-induced torques, showing that currents are much more efficient than magnetic fields for the switching of AFMs.

After optimizing the epitaxial CoO/Pt thin film growth [22–24], we first probe electrically the magnetic anisotropy of the CoO by means of uniaxial field-sweep magnetoresistive (MR) scans and angularly detected

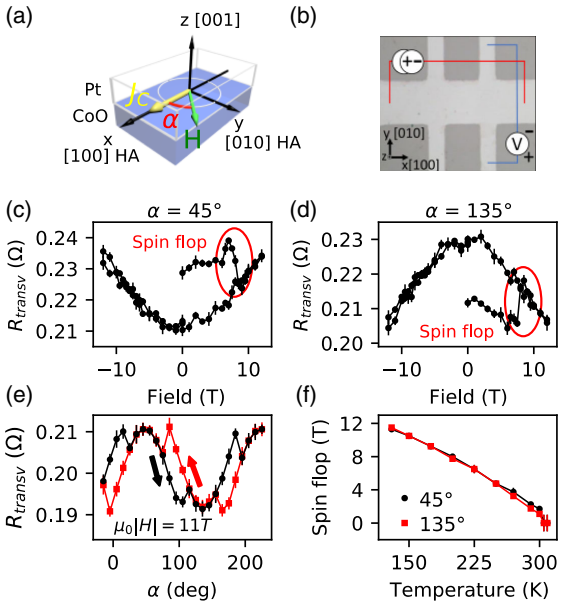

FIG. 1. Magnetic anisotropy of the CoO thin films. (a) Coordinate system. (b) Optical micrograph of one Hall bar and contact scheme. (c) Field-induced spin flop at 200 K, read by SMR in the presence of a field applied along the [110] direction ($\alpha = 45°$) in CoO(5 nm)/Pt(2 nm). A 12 T field was previously applied along the orthogonal direction. (d) Field-induced spin flop with orthogonal field direction compared to the previous one. (e) Transverse ADMR scans showing hysteresis loops associated with the spin-flop transition. (f) Spin-flop field versus temperature, yielding $T_{\text{Néel}=305\pm5\ \text{K}}$.

magnetoresistance (ADMR) scans in patterned Hall bar devices 10 μm wide, orientated along the [100] direction [20,21,25,26]. The electrical measurements were performed in a cryostat, equipped with a variable temperature insert, a rotating sample stage, and a superconducting magnet generating fields up to 12 T. The orientation of $\boldsymbol{n}$ can be read electrically, by means of the transverse SMR signal, proportional to the in-plane Néel vector components $n_x * n_y$, according to the geometry shown in Figs. 1(a) and 1(b). Note that the SMR is maximized when two states with orthogonal orientation of $\boldsymbol{n}$ are present in the system. The resistance was measured by a Keithley 2400 and a Keithley 2182A and averaged between opposite dc current polarities, with a density of $j_{\text{meas}} \sim 5 \times 10^9$ A m^{-2}, thus minimizing thermally induced electric effects, similar to the protocol developed for antiferromagnetic hematite [27]. When the field is applied alternating along the [110] or $[\bar{1}10]$ directions (easy axes) at 200 K, we find at 8 T an abrupt spin-flop transition in a MgO(001)//CoO(5 nm)/Pt(2 nm) sample, as shown in Figs. 1(c) and 1(d). The resistance change at the spin flop is consistent with a negative sign of the SMR [20,21,25,26]. Moreover, applying a field along the [001] out-of-plane direction (hard axis) does not lead to a spin flop below 12 T at 200 K, in line with a biaxial in-plane magnetic anisotropy. We did not find a hysteresis loop signature in the MR scans, showing that the CoO(001) interface is likely fully compensated [14]. By looking at the ADMR scan in Fig. 1(e), one can see a $\sin^2(\alpha + \alpha_0)$ signal [23] and three distinct hysteresis loops, centered around the $\alpha = 0°[100]$, $\alpha = 90°[010]$, and $\alpha = 180°[\bar{1}00]$ directions (hard axes), while the resistance is not hysteretic around the $\alpha = 45°$ and $\alpha = 135°$ (easy axes). The hysteresis loops, according to a macrospin model (Supplemental Material [22]), are due to the lag of $\boldsymbol{n}$ behind the rotation of $\boldsymbol{H}$ in the vicinity of the hard axes (HAs), while we observe field-induced spin flop of $\boldsymbol{n}$ in the vicinity of the two orthogonal in-plane easy axes (EAs). These observations demonstrate the fourfold in-plane magnetic anisotropy of the CoO layer induced by the strain, with an out-of-plane hard axis along the [001] direction and two easy axes in the (001) plane ([110] and $[\bar{1}10]$), in agreement with the symmetry of the anisotropy conjectured in exchange-biased CoO/Fe thin films [19]. Moreover, we show in Fig. 1(f) that the spin-flop field vanishes at $T_{\text{Néel}} = 305 \pm 5$ K. This is increased by 10 K compared to the bulk due to strain [17], in line with the literature.

Next we need to ascertain that we can obtain current-induced switching in the fourfold CoO thin films. We use eight-arm Hall star devices with measuring arms 2 μm wide and pulsing arms 10 μm wide. The pulsing arms, where the current flows, are orientated along the [110] and $[\bar{1}10]$ easy axes directions [Figs. 2(a)–2(d)] at 200 K. To set a well-defined starting state, we applied $\mu_0 H_{\text{before}} = 11$ T

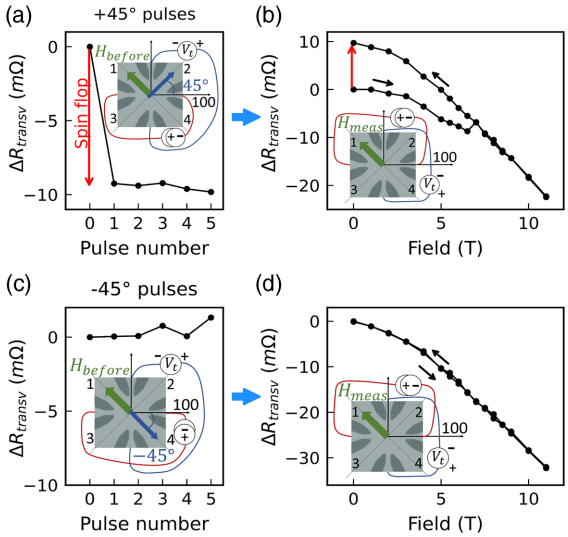

FIG. 2. Symmetry of the current-induced switching. (a) $\mu_0 H_{\text{before}} = 11$ T was applied along the 4-1 contacts direction $[\bar{1}10]$ to align the Néel vector $\boldsymbol{n}$ along 3-2 [110] and then removed. A steplike switching by pulses along 3-2 (starting state $\boldsymbol{j}_{\text{pulse}} \| \boldsymbol{n}$) is seen, corresponding to a current-induced spin-flop transition of $\boldsymbol{n}$ along 4-1 (final state $\boldsymbol{j}_{\text{pulse}} \perp \boldsymbol{n}$). (b) The MR scan with field along 4-1 shows a field-induced spin flop, which resets $\boldsymbol{n}$ along 3-2. (c),(d) No switching or spin flop are observed by pulses $\boldsymbol{j}_{\text{pulse}} \perp \boldsymbol{n}$, as this is already the final state.

along the $[\bar{1}10]$ direction, i.e., along the 4-1 contacts direction, as defined in the inset of Fig. 2(a), and then reduced the field to 0 T, thus aligning before each pulse $\boldsymbol{n}\perp\boldsymbol{H}$ along the in-plane direction of the 3-2 contacts ([110]). In the case of Fig. 2(a), we applied five pulses 1 ms long and with a current density of $j_{\mathrm{pulse}} = 1.15 \times 10^{12}$ A m^{-2} along the 3-2 contacts direction (initial state $\boldsymbol{n}\|\boldsymbol{j}_{\mathrm{pulse}}$) by a Keithley 6221; i.e., the pulses were applied with $\boldsymbol{j}_{\mathrm{pulse}}\perp\boldsymbol{H}_{\mathrm{before}}$. The transverse resistance, measured 10 s after the application of the pulses, drops after the first pulse, in a steplike fashion that was also reported in NiO/Pt [4,6], indicating a current-induced 90° $\boldsymbol{n}$ rotation analogous to the spin-flop transition. If one performs a MR scan with field along the 4-1 contacts direction after the current pulses, shown in Fig. 2(b), one observes a field-induced spin-flop transition of $\boldsymbol{n}$ back to the initial state (along [110]). Note that the height of the current-induced switching in Fig. 2(a) (red arrow) and of the field-induced spin flop in Fig. 2(b) (red arrow) are identical within the error and have the same magnitude as the spin flop induced by a field only (Supplemental Material [22]), suggesting that both fields and currents switch $\boldsymbol{n}$ equivalently. From the presence of a spin flop after the 3-2 current pulse [Fig. 2(b)], considering that a spin flop occurs only when $\boldsymbol{H}\|\boldsymbol{n}$, we determine that the switching final state is $\boldsymbol{n}\perp\boldsymbol{j}_{\mathrm{pulse}}$. Accordingly, if after applying a field along $[\bar{1}10]$, five current pulses are applied along the same direction 1-4 $[1\bar{1}0]$, no transverse resistance variation and subsequent spin-flop transition are seen in the field scan [Figs. 2(c) and 2(d)], as in this case the initial state $\boldsymbol{n}\perp\boldsymbol{j}_{\mathrm{pulse}}$ is already coincident with the final state observed after a current pulse. The switching can be reversed by sending current pulses along alternating orthogonal pulsing arms of the device, in the absence of any field. We show in the Supplemental Material [22] approximately 350 current-induced switching events, without breaking the device. The current pulse polarity does not play a detectable role for the switching. These results confirm unambiguously the electrical reading and writing of the orientation of $\boldsymbol{n}$ in AFMs.

Finally, to quantify the current-field equivalence in the CoO(5 nm)/Pt system, we study the current-induced switching in the presence of static magnetic fields, applied along or perpendicular to the initial $\boldsymbol{n}$ of the system, during the current pulse. In Fig. 3(a) we show an example of this

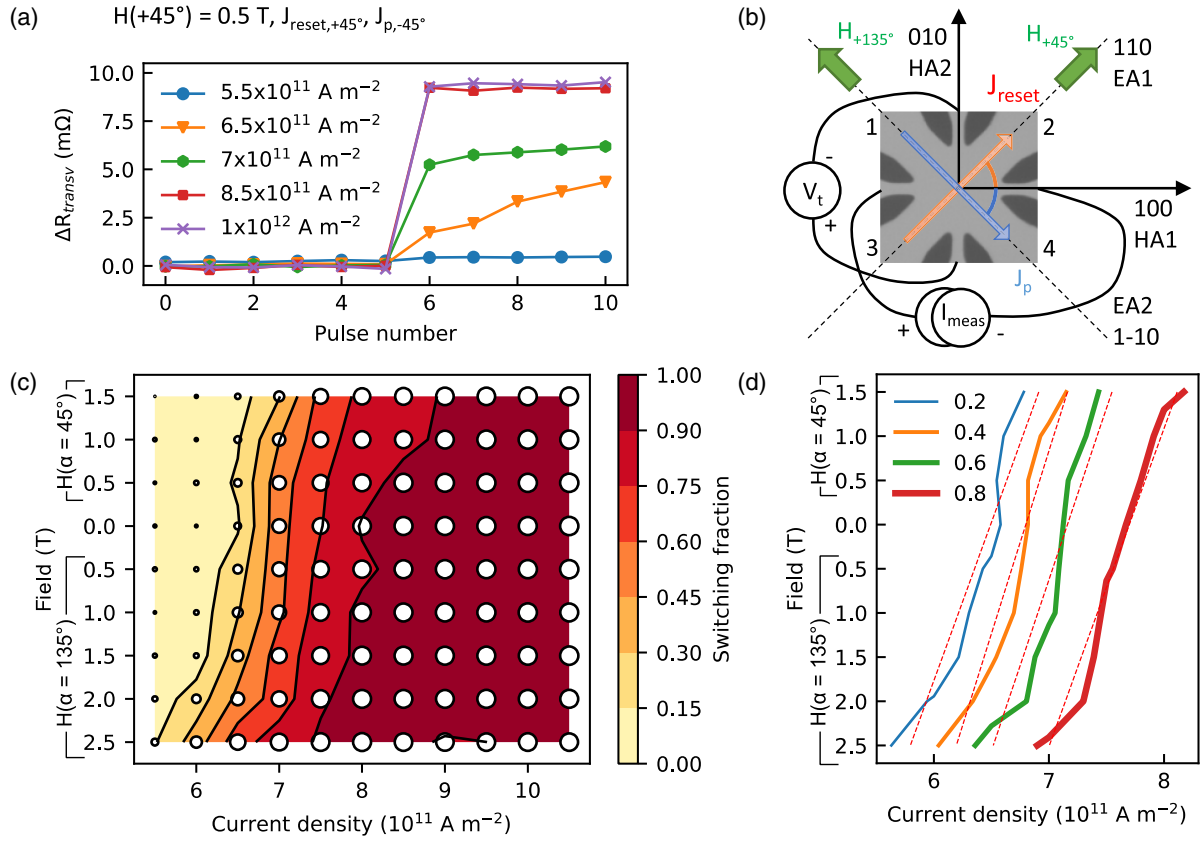

FIG. 3. (a) Transverse resistance variation versus pulse current density, probing the threshold and saturation of the switching. Before the measurements, a reset pulse ($j_{\mathrm{reset}} = 1.05 \times 10^{12}$ A m^{-2}) was applied along 3-2, followed by five pulses along 3-2 and five pulses along 1-4. (b) Scheme of the measurements. (c) Switching fraction as a function of the applied field and pulse current. The circles represent the data points; the lines are contour plots with constant switching efficiency. (d) Current-field equivalence obtained by linear fits of the contour plots from the data in Fig. 3(c) for different switching fractions.

type of measurements for a single field, where we prepare the system in the same reproducible starting state with a reset pulse along 3-2 of current density $j_{\mathrm{reset}} = 1.05 \times 10^{12}\ \mathrm{A\,m^{-2}}$ and vary j_{pulse} of the subsequent pulses along 1-4, as shown in Fig. 3(b). By the saturation level of the transverse resistance, we can determine the switching fraction assuming it is proportional to the resistance increase and normalized to 100% at saturation. The amplitude of the switching as a function of the pulse current and field is shown in Fig. 3(c), where the color indicates the switching fraction (the darker the color, the higher the fraction). The main result is that both the threshold and the saturation current are increased (decreased) if the field is applied orthogonal (parallel) to the initial orientation of $\boldsymbol{n}$. This is consistent with the fact that the Zeeman energy is minimum in antiferromagnets when $\boldsymbol{H} \perp \boldsymbol{n}$ [21]. By interpolation of the data, we can obtain the contour plots of equal switching efficiency that can be fitted by linear functions having R^2 values larger than 0.87, thus indicating that a linear relation between the field and the current can explain the data well. From the fits and considering the geometry of the device, we obtain a current-field equivalence of $4 \times 10^{-11}\ \mathrm{T\,A^{-1}\,m^2}$, several orders of magnitude larger than the value of $10^{-15}\ \mathrm{T\,A^{-1}\,m^2}$ obtained for typical ferro(i)magnetic insulators, such as TIG/Pt [28]. The switching current density at zero field in CoO/Pt is $j_{\mathrm{pulse}} = 6.5 \times 10^{11}\ \mathrm{A\,m^{-2}}$ for a switching fraction of 15% and $j_{\mathrm{pulse}} = 8.5 \times 10^{11}\ \mathrm{A\,m^{-2}}$ to achieve a full switching, similar to what is found in TIG/Pt [29]. This shows that the obtained giant current-field equivalence ratio results from a current-induced switching that is equally efficient as in ferro(i)magnetic insulators, while the field-induced switching is very inefficient due to the insensitivity of AFMs against external magnetic fields. Note that we find a similar order of magnitude if we use a second method to estimate the current-field equivalence, namely, by switching with pulses of increasing current density and looking at the increasing spin-flop field of the switched states (Supplemental Material [22]).

To understand the field-current equivalence of the torques and the occurring switching mechanism, we consider the different torque mechanisms proposed to date: the dampinglike spin-orbit torques (SOTs) acting on uncompensated ferromagnetic spins [4], dampinglike SOTs acting on the antiferromagnetic sublattices [5,6], and the thermomagnetoelastic effects [7]. The SOT switching mechanism related to uncompensated interfacial spins [4] cancels out in our sputtered films with CoO(001) surfaces with a compensated checkerboard alignment of the spins [14] and the expected roughness and atomic steps. The mechanism based on SOTs in AFMs is related to the spin accumulation induced by the spin Hall effect [5]. The corresponding SOTs create staggered fields, which remove the degeneracy between the two orthogonal orientations of $\boldsymbol{n}$, leading to a current-induced energy term competing with the magnetic anisotropy [6],

$$w_{\mathrm{SOT}} = -\frac{\varepsilon^2}{H_{\parallel} M_s} (\boldsymbol{n} \cdot \boldsymbol{j}_{\mathrm{pulse}})^2, \tag{1}$$

where $H_{\parallel} > 0$ is the out-of-plane magnetic anisotropy of CoO, and ε is a material-dependent constant that parametrizes the coupling between the spin current and the localized moments of the CoO layer. To minimize this contribution, the predicted final state of the switching is $\boldsymbol{n} \| \boldsymbol{j}_{\mathrm{pulse}}$, opposite of what we probe. By comparing the expression (1) to the effective Zeeman energy contribution of the magnetic field

$$w_{\mathrm{Zee}} = H_j H_k (n_j n_k - \delta_{jk}) / H_{\mathrm{ex}}, \tag{2}$$

where H_{ex} is the exchange field, H_{jk} are the external field components. We conclude that the spin-polarized current is linearly proportional to the effective magnetic field generated by the torque $\boldsymbol{H}_{\mathrm{SOT}} \propto \hat{\boldsymbol{z}} \times \boldsymbol{j}_{\mathrm{pulse}}$.

The third possible mechanism is related to Joule heating. It results from the combined effect of thermal expansion and magnetoelasticity [7]. According to this model, the degeneracy of the orthogonal states can be removed by the magnetoelastic contribution $w_{\mathrm{me}} = \lambda u_{jk}^{\mathrm{rel}} n_j n_k$ into the magnetic energy, where λ is the magnetoelastic constant. The shear strains $u_{jk}^{\mathrm{rel}}(\mathbf{r})$ compensate the stresses induced by the incompatibility of the thermal lattice (volume) expansion along the lines that separate high and low temperature regions. The strains along the direction of temperature gradient are tensile at the hotter side and are compressive at the colder side. In the center of the structure (where we read the SMR signal), the overall strain is compressive along the current direction (Supplemental Material [22]). The absolute value of the strain is proportional to the temperature gradient, but, in general, depends on the temperature distribution in the whole sample due to the nonlocality of the elastic interactions. However, as the temperature gradient is induced by Joule heating, $u_{jk}^{\mathrm{rel}} \propto j_{\mathrm{pulse}}^2$. Hence, in this region the current-induced contribution into the magnetic energy scales as

$$w_{\mathrm{me}} \propto -\lambda (\boldsymbol{n} \cdot \boldsymbol{j}_{\mathrm{pulse}})^2. \tag{3}$$

Assuming that the sign of the magnetoelastic constant in CoO is $\lambda < 0$ [30], the elongation in the direction of $\boldsymbol{n}$ is favored, which yields a final state $\boldsymbol{n} \perp \boldsymbol{j}_{\mathrm{pulse}}$, resulting from the competition of pure magnetic and magnetoelastic anisotropies. Note that, in a general case, the strains $u_{jk}^{\mathrm{rel}}(\mathbf{r})$ depend on the distribution of the current density gradients with respect to the observation point and are not directly related to the direction of $\boldsymbol{j}_{\mathrm{pulse}}$, in contrast to the case of SOTs. If we compare w_{me} and w_{Zee}, one can see that the value of the effective magnetic field generated by

thermomagnetoelastic effects is $H_{me} \propto j_{pulse}$, while its orientation is sensitive to the geometry of the experiment and can be either parallel or perpendicular to the current direction.

Overall, both models predict a linear dependence of the effective field on the current density, as found experimentally. The final state after switching, found here in the discussion of Fig. 2 ($\boldsymbol{n} \perp \boldsymbol{j}_{pulse}$), is consistent with the final state expected from switching by the thermomagnetoelastic mechanism found in α-Fe_2O_3/Pt [7] and is opposite of the final state expected from switching due to an antiferromagnetic antidampinglike interfacial spin-orbit torque ($\boldsymbol{n} \| \boldsymbol{j}_{pulse}$) [5,6,9]. While both SOT and thermomagnetoelastic effects might be present, here the thermomagnetoelastic mechanism dominates. However, knowing the sign of the magnetostriction of CoO thin films is required to confirm that this mechanism leads to the observed final state of the switching, which has not been reported up to now in thin films. This thermomagnetoelastic mechanism can be stronger in CoO compared to other materials due to the large magnetostriction on the order of 10^{-3} [31,32] and large out-of-plane magnetic anisotropy in our in-plane thin film samples, which can overcome the switching mechanism based on SOT effects in this material [6]. Also note that the combination of Eqs. (2) and (3) explains the dependence on the field orientation that we found experimentally: when $\boldsymbol{H} \| \boldsymbol{j}_{pulse}$ [$\alpha = 135°$ in Figs. 3(c) and (d)], the two energy terms act constructively to decrease the current-switching threshold, while when $\boldsymbol{H} \perp \boldsymbol{j}_{pulse}$ ($\alpha = 45°$), the current-switching threshold is increased (Supplemental Material [22]).

In conclusion, we report here the measured equivalence of current and field in antiferromagnetic CoO/heavy metal Pt bilayers, where the CoO is antiferromagnetic and has the fourfold in-plane anisotropy, which can be ideal for applications. First, our data clearly show that electrical reading and writing of the switching in antiferromagnetic materials is possible and achieved efficiently in CoO/Pt. Second, we find that the relation between current and field is linear and of magnitude much larger than in ferromagnets, with current-induced switching similarly efficient as in ferromagnets and the insensitivity of the AFMs against external magnetic fields. Third, the switching final state and current-field equivalence suggest that a switching mechanism based on thermomagnetoelastic effects is the likely origin of the observed switching.

The authors thank A. Ross, J. Henrizi, A. Dion, and T. Reimer for skillful technical assistance. L. B. acknowledges the European Union's Horizon 2020 research and innovation program under the Marie Skłodowska-Curie Grant agreements ARTES No. 793159. O. G. acknowledges the EU FET Open RIA Grant No. 766566, the DFG (project SHARP 397322108), and that this work was funded by the Deutsche Forschungsgemeinschaft (DFG, German Research Foundation)—TRR 288—422213477 (project A09). L. B., R. L., and M. K. acknowledge support from the Graduate School of Excellence Materials Science in Mainz (MAINZ) DFG 266, the DAAD (Spintronics network, Project No. 57334897), and all groups from Mainz acknowledge that this work was Funded by the Deutsche Forschungsgemeinschaft (DFG, German Research Foundation)—TRR 173–268565370 (projects A01, A03, A11, B02, and B12). We acknowledge financial support from the Horizon 2020 Framework Programme of the European Commission under FET-Open Grant Agreement No. 863155 (s-Nebula). This project has received funding from the European Research Council (ERC) under the European Union's Horizon 2020 research and innovation programme under Grant Agreement No. 856538. J. S. acknowledges support from the Grant Agency of the Czech Republic Grant No. 19-28375X and ASPIN EU FET Open RIA Grant No. 766566. This work was also supported by ERATO "Spin Quantum Rectification Project" (Grant No. JPMJER1402) and the Grant-in-Aid for Scientific Research on Innovative Area, "Nano Spin Conversion Science" (Grant No. JP26103005), Grant-in-Aid for Scientific Research (S) (Grant No. JP19H05600) from JSPS KAKENHI, R. R. also acknowledges support by Grant-in-Aid for Scientific Research (C) (Grant No. JP20K05297), from JSPS KAKENHI, Japan. R. L. acknowledges the European Union's Horizon 2020 research and innovation program under the Marie Skłodowska-Curie Grant agreement FAST No. 752195.

*lbaldrat@uni-mainz.de
†Klaeui@Uni-Mainz.de

[1] V. Baltz, A. Manchon, M. Tsoi, T. Moriyama, T. Ono, and Y. Tserkovnyak, Rev. Mod. Phys. **90**, 015005 (2018).
[2] P. Wadley *et al.*, Science **351**, 587 (2016).
[3] S. Y. Bodnar, L. Šmejkal, I. Turek, T. Jungwirth, O. Gomonay, J. Sinova, A. A. Sapozhnik, H. J. Elmers, M. Kläui, and M. Jourdan, Nat. Commun. **9**, 348 (2018).
[4] T. Moriyama, K. Oda, T. Ohkochi, M. Kimata, and T. Ono, Sci. Rep. **8**, 14167 (2018).
[5] X. Z. Chen, R. Zarzuela, J. Zhang, C. Song, X. F. Zhou, G. Y. Shi, F. Li, H. A. Zhou, W. J. Jiang, F. Pan, and Y. Tserkovnyak, Phys. Rev. Lett. **120**, 207204 (2018).
[6] L. Baldrati, O. Gomonay, A. Ross, M. Filianina, R. Lebrun, R. Ramos, C. Leveille, F. Fuhrmann, T. R. Forrest, F. Maccherozzi, S. Valencia, F. Kronast, E. Saitoh, J. Sinova, and M. Klaüi, Phys. Rev. Lett. **123**, 177201 (2019).
[7] P. Zhang, J. Finley, T. Safi, and L. Liu, Phys. Rev. Lett. **123**, 247206 (2019).
[8] I. Gray, T. Moriyama, N. Sivadas, G. M. Stiehl, J. T. Heron, R. Need, B. J. Kirby, D. H. Low, K. C. Nowack, D. G. Schlom, D. C. Ralph, T. Ono, and G. D. Fuchs, Phys. Rev. X **9**, 041016 (2019).
[9] Y. Cheng, S. Yu, M. Zhu, J. Hwang, and F. Yang, Phys. Rev. Lett. **124**, 027202 (2020).

[10] T. Matalla-Wagner, J.-M. Schmalhorst, G. Reiss, N. Tamura, and M. Meinert, Phys. Rev. Research **2**, 033077 (2020).
[11] C. C. Chiang, S. Y. Huang, D. Qu, P. H. Wu, and C. L. Chien, Phys. Rev. Lett. **123**, 227203 (2019).
[12] A. Churikova, D. Bono, B. Neltner, and A. Wittmann, Appl. Phys. Lett. **116**, 022410 (2020).
[13] E. Uchida, N. Fukuoka, H. Kondoh, T. Takeda, Y. Nakazumi, and T. Nagamiya, J. Magn. Soc. Jpn. **19**, 2088 (1964).
[14] W. L. Roth, Phys. Rev. **110**, 1333 (1958).
[15] S. Saito, K. Nakahigashi, and Y. Shimomura, J. Phys. Soc. Jpn. **21**, 850 (1966).
[16] K. Inagawa, K. Kamigaki, and S. Miura, J. Phys. Soc. Jpn. **31**, 1276 (1971).
[17] S. I. Csiszar, M. W. Haverkort, Z. Hu, A. Tanaka, H. H. Hsieh, H. J. Lin, C. T. Chen, T. Hibma, and L. H. Tjeng, Phys. Rev. Lett. **95**, 187205 (2005).
[18] J. Zhu, Q. Li, J. X. Li, Z. Ding, J. H. Liang, X. Xiao, Y. M. Luo, C. Y. Hua, H. J. Lin, T. W. Pi, Z. Hu, C. Won, and Y. Z. Wu, Phys. Rev. B **90**, 054403 (2014).
[19] W. N. Cao, J. Li, G. Chen, J. Zhu, C. R. Hu, and Y. Z. Wu, Appl. Phys. Lett. **98**, 262506 (2011).
[20] H. Nakayama, M. Althammer, Y. T. Chen, K. Uchida, Y. Kajiwara, D. Kikuchi, T. Ohtani, S. Geprägs, M. Opel, S. Takahashi, R. Gross, G. E. W. Bauer, S. T. B. Goennenwein, and E. Saitoh, Phys. Rev. Lett. **110**, 206601 (2013).
[21] L. Baldrati, A. Ross, T. Niizeki, C. Schneider, R. Ramos, J. Cramer, O. Gomonay, M. Filianina, T. Savchenko, D. Heinze, A. Kleibert, E. Saitoh, J. Sinova, and M. Kläui, Phys. Rev. B **98**, 024422 (2018).
[22] See Supplemental Material at http://link.aps.org/supplemental/10.1103/PhysRevLett.125.077201 for the growth and magnetic characterization of the CoO films, macrospin model of the field-induced switching, comparison between the field- and current-induced switching, switching reproducibility, and derivation of the current-field equivalence equations for the thermomagnetoelastic mechanism. This material includes Refs. [7,14,23,24]
[23] K. Oda, T. Moriyama, M. Kimata, S. Kasukawa, and T. Ono, Jpn. J. Appl. Phys. **59**, 010908 (2020).
[24] M. Isasa, S. Vélez, E. Sagasta, A. Bedoya-Pinto, N. Dix, F. Sánchez, L. E. Hueso, J. Fontcuberta, and F. Casanova, Phys. Rev. Applied **6**, 034007 (2016).
[25] G. R. Hoogeboom, A. Aqeel, T. Kuschel, T. T. M. Palstra, and B. J. van Wees, Appl. Phys. Lett. **111**, 052409 (2017).
[26] J. Fischer, O. Gomonay, R. Schlitz, K. Ganzhorn, N. Vlietstra, M. Althammer, H. Huebl, M. Opel, R. Gross, S. T. B. Goennenwein, and S. Geprägs, Phys. Rev. B **97**, 014417 (2018).
[27] R. Lebrun, A. Ross, O. Gomonay, S. A. Bender, L. Baldrati, F. Kronast, A. Qaiumzadeh, J. Sinova, A. Brataas, R. A. Duine, and M. Kläui, Commun. Phys. **2**, 50 (2019).
[28] S. Ding, A. Ross, R. Lebrun, S. Becker, K. Lee, I. Boventer, S. Das, Y. Kurokawa, S. Gupta, J. Yang, G. Jakob, and M. Kläui, Phys. Rev. B **100**, 100406(R) (2019).
[29] C. O. Avci, A. Quindeau, C. F. Pai, M. Mann, L. Caretta, A. S. Tang, M. C. Onbasli, C. A. Ross, and G. S. D. Beach, Nat. Mater. **16**, 309 (2017).
[30] T. R. McGuire and W. A. Crapo, J. Appl. Phys. **33**, 1291 (1962).
[31] J. Kanamori, Prog. Theor. Phys. **17**, 197 (1957).
[32] Y. Narumi, K. Katsumata, U. Staub, K. Kindo, M. Kawauchi, C. Broennimann, H. Toyokawa, Y. Tanaka, A. Kikkawa, T. Yamamoto, M. Hagiwara, T. Ishikawa, and H. Kitamura, J. Phys. Soc. Jpn. **75**, 075001 (2006).

Correction: For compliance purposes, more specific wording was added in the Acknowledgments section for the s-Nebula project.